Supplementary Information

Bio-inspired hydrogel with high ionic conductivity and tissue-like flexibility for bioelectronics

Baojin Chen,[1] Renjie Yu,[1] Jiaqi Wang,[1] Yunxiang Feng,[1] Yujie Zhang,[1] Yanchao Mao,[1,*] Chongxin Shan,[1,*] Xudong Wang[2,*]

[1]Key Laboratory of Materials Physics of Ministry of Education, School of Physics, Zhengzhou University, Zhengzhou 450001, China

* E-mail: ymao@zzu.edu.cn; cxshan@zzu.edu.cn

[2]Department of Materials Science and Engineering, University of Wisconsin-Madison, Madison, WI 53706, USA

* Email: xudong@engr.wisc.edu

Supplementary Note 1. The calculating process of EIS measurement and the related fitting results.

To characterize the electrical properties of hydrogels, Nyquist plots were obtained through the EIS measurement. A constant phase element (CPE) modified Randles equivalent circuit model noted as the Randles-CPE model was established to analyze the electrochemical processes. This model incorporates a CPE to account for the non-ideal behavior of resistive, capacitive, and other electrochemical components in the system. The schematic diagram of the Randles-CPE equivalent circuit is shown in the set of Fig 2a. According to the equivalent circuit model, the total impedance of the system can be expressed as

$$Z = R_s + Z_{interface} \quad (1)$$

In this equation, R_s represents the bulk resistance of the hydrogel, reflecting its intrinsic electrical conductivity and high-frequency impedance. $Z_{interface}$ consists of a double-layer capacitance (C_d) and a faradaic impedance (Z_f) connected in parallel. In the Nyquist plot, R_s corresponds to the intersection of the high-frequency region with the real axis. Z_f consists the charge transfer resistance (R_{ct}) and the impedance of the constant phase element (Z_{CPE}) connected in series. The $Z_{interface}$ can be further expressed as

$$Z_{interface} = \frac{1}{\frac{1}{R_{ct}+Z_{CPE}}+jwC_d} \quad (2)$$

Here, R_{ct} is the charge transfer resistance at the hydrogel-electrode interface, directly reflecting the kinetics of the faradaic process. Meanwhile, Z_{CPE} accounts for non-ideal behavior of the electrode surface, such as the influence of surface roughness or defects on impedance.

The impedance of the CPE can be mathematically described as

$$Z_{CPE} = \frac{1}{(jw)^{\alpha}Y_0} \quad (3)$$

In this equation, Y_0 is the CPE constant, which is influenced by the electrolyte properties, interface structure, and material characteristics, and significantly affects the

impedance magnitude at low frequencies. w is the angular frequency, defined as $w=2\pi f$, and f is the frequency. The exponent α characterizes the phase angle behavior of the system, with values ranging between 0 and 1. When $\alpha = 1$, the CPE behaves as an ideal capacitor, and its impedance becomes $Z_{CPE} = \frac{1}{jwC}$, representing purely capacitive behavior. Conversely, when $\alpha = 0$, the CPE acts as an ideal resistor, with its impedance expressed as $Z_{CPE} = R$. For intermediate values (0<α<1), the CPE exhibits a hybrid impedance behavior that blends capacitive and resistive characteristics. By combining the equations (1), (2), and (3), the overall impedance of the circuit can be expressed as

$$Z = R_S + \frac{R_{ct}(jw)^{\alpha}Y_0+1}{(jw)^{\alpha}Y_0+jwC_d[\mathrm{R_{ct}}(jw)^{\alpha}\mathrm{Y_0}+1]} \quad (4)$$

This equation provides a complete representation of the system's impedance, incorporating both the bulk resistance of the hydrogel and the complex impedance.

During the EIS measurement, an alternating current signal with varying frequencies is applied to the system, and the total impedance is expressed as

$$Z = Z_{real} + j \cdot Z_{im} \quad (5)$$

where Z_{real} represents the real part of the impedance, which corresponds to the resistive component , while Z_{im} represents the imaginary part, which corresponds to the capacitive or inductive component. The imaginary unit j is defined by $j^2 = -1$. In the Nyquist plot, Z_{real} is plotted on the horizontal axis, and Z_{im} on the vertical axis. The Nyquist curve can be obtained by plotting the relationship between Z_{real} and Z_{im} at different frequencies, as shown in Fig 1d, 2a, and 2b. The corresponding fitting results of these Nyquist curves are summarized in Tables S1, S2, and S3. Then, the electrical conductivity (σ) of the hydrogel can be calculated using the following equation

$$\sigma = \frac{L}{SR_s} \quad (6)$$

In this equation, L is the thickness of the hydrogel, and S is its cross-sectional area. In this study, $L = 0.0025$ m and $S = 0.0001$ m². This formula directly correlates the bulk resistance of the hydrogel to its conductivity, providing a quantitative evaluation

of its electrical property.

Supplementary Table 1. Fitting parameters for the EIS measurements of different monomer based hydrogels (Fig. 1d).

Monomer	Sample	R_s (Ω)	Y_0 ($\mu S \cdot s^{\alpha}$)	α	R_{ct} (Ω)	C_d (μF)	σ ($S \cdot m^{-1}$)
SMBA	1	3.47	25.0	0.78	28.23	12.5	7.20
	2	3.54	24.3	0.78	26.90	12.5	7.06
	3	3.64	26.3	0.78	26.87	11.9	6.86
DMA	1	11.59	13.7	0.79	23.36	4.5	2.15
	2	12.17	13.7	0.79	23.09	4.6	2.05
	3	12.93	14.2	0.80	16.44	3.3	1.93
EMA	1	14.74	16.5	0.77	19.43	3.6	1.70
	2	14.14	14.9	0.78	18.37	2.9	1.77
	3	14.25	14.2	0.78	18.81	3.1	1.75
HEAA	1	15.77	8.67	17.48	17.48	1.9	1.59
	2	16.13	8.69	18.46	18.46	2.0	1.55
	3	16.16	8.69	18.69	18.69	2.0	1.55

Supplementary Table 2. Fitting parameters for the EIS measurements of BIH with different LiCl electrolyte content (Fig. 2a).

Content	Sample	R_s (Ω)	Y_0 ($\mu S \cdot s^{\alpha}$)	α	R_{ct} (Ω)	C_d (μF)	σ ($S \cdot m^{-1}$)
3.07 wt%	1	3.47	25.0	0.78	28.23	12.5	7.20
	2	3.54	24.3	0.78	26.90	12.5	7.06
	3	3.64	26.3	0.78	26.87	11.9	6.86
2.47 wt%	1	5.32	31.0	0.78	17.09	8.4	4.69
	2	5.19	29.9	0.78	16.93	8.6	4.81
	3	5.62	21.1	0.79	20.90	8.1	4.45
	1	6.19	21.6	0.78	23.50	7.7	4.03

1.87 wt%	2	6.30	21.2	0.78	24.17	7.8	3.97
	3	6.35	20.8	0.78	24.42	7.8	3.93
1.25 wt%	1	9.66	21.6	0.78	29.10	7.9	2.59
	2	9.83	21.2	0.78	24.75	7.7	2.54
	3	9.91	20.8	0.78	25.87	7.7	2.52
0.63 wt%	1	16.58	19.8	0.77	24.09	6.8	1.51
	2	17.01	19.6	0.77	22.60	6.5	1.47
	3	17.15	19.5	0.77	23.10	6.5	1.46

Supplementary Table 3. Fitting parameters for the EIS measurements of BIH with different electrolyte types (Fig. 2b).

Electrolyte	Sample	R_s (Ω)	Y_0 ($\mu S \cdot s^{\alpha}$)	α	R_{ct} (Ω)	C_d (μF)	σ ($S \cdot m^{-1}$)
LiCl	1	6.19	21.6	0.78	23.50	7.7	4.03
	2	6.30	21.2	0.78	24.17	7.8	3.96
	3	6.35	20.8	0.78	24.42	7.8	3.94
KCl	1	6.46	22.1	0.76	23.86	6.2	3.87
	2	6.37	25.4	0.76	23.20	6.8	3.92
	3	6.49	24.7	0.76	24.36	6.9	3.85
NH_4Cl	1	6.91	21.0	0.77	24.14	6.5	3.62
	2	7.07	20.3	0.77	25.43	6.5	3.54
	3	7.12	20.1	0.77	25.33	6.5	3.51
NaCl	1	7.34	24.6	0.76	20.96	6.7	3.41
	2	7.50	23.9	0.76	23.32	6.8	3.33
	3	7.57	23.1	0.76	23.13	6.8	3.30
LiBr	1	9.27	18.8	0.78	18.39	5.9	2.70
	2	9.44	18.2	0.78	21.23	6.1	2.65
	3	9.48	17.9	0.78	21.89	6.2	2.64

Supplementary Note 2. The calculation process of the SNR for ECG and EMG signals

To evaluate the performance of BIH electrodes in electrophysiological monitoring, the SNR of the electrophysiological signals was calculated. A Butterworth low-pass filter was applied for ECG signal processing. The squared amplitude of the transfer function is expressed as

$$|H(jw)|^2 = \frac{1}{1+\left(\frac{w}{w_c}\right)^{2N}} \quad (7)$$

Where ω_c represents the 3 dB cut-off frequency, and N denotes the filter order. The cut-off frequency ω_c was set to 30 Hz and the filter N=3 are used, and the sampling frequency is 10000 Hz. The transfer function of the filter was derived through MATLAB simulation, yielding the following equation

$$H(z) = \frac{V_{signal}(z)}{V(z)} = \frac{8.22+24.65z^{-1}+24.65z^{-2}+8.22z^{-3}}{1-2.96z^{-1}+2.93z^{-2}-0.96z^{-3}} \times 10^{-7} \quad (8)$$

Where $Z=e^{j\omega}$, V and V_{signal} represent the z-transform of the ECG signal sequence v and v_{signal} before and after filtering. From the equation (8), the filtered signal v_{signal} can be derived from v. The difference between the ECG signal before and after filtering is considered as noise, and the SNR of ECG signal is calculated using the following equation

$$SNR_{ECG} = 10log_{10}\frac{|v_{signal}|^2}{|v-v_{signal}|^2} \quad (9)$$

During the measurement process of the EMG signal, the muscle operates in both resting and active states. The signals from these two states are relatively stable and distinctly identifiable. To calculate the SNR, the two states are separated, and the noise power is calculated using the EMG signal power from the resting state. Initially, the collected electrical signals are divided into r data groups. The i-th group of data can be expressed as

$$\{v_{i1}\} = \{v_{i1}, v_{i2}, \ldots, v_{ir}\}, \mathrm{i} = 1,2,\ldots,\frac{N}{r} \quad (10)$$

where N is the sample number of the electrical signal sequence v. In this study, N is about 60000 data points, and $r = 10$ is considered. For each data group, the average power is calculated as

$$P_i = \frac{1}{10}\sum_{j=1}^{10} v_{ij}^2 \quad (11)$$

Then, the frequency distribution histogram of $\log_{10}P_i$ is drawn as shown in Fig S8. The number of groups is $Nbins = 60$. The data corresponding to each group is represented as

$$bins\,(k) = (k-\frac{1}{2})\frac{\max(log_{10}^{P_i}) - \min(\log)}{Nbins} + \min(\log_{10}^{P_i}) \quad (12)$$

where, $k = 1,2,\ldots,Nbins$. The histogram reveals two distinct peaks, corresponding to the varying power of the EMG signal during the resting and active states. The left peak represents the signal in the resting state, while the right peak corresponds to the active state, exhibiting clear differentiation between the two conditions. It is hypothesized that the noise power of the signal aligns with the signal power measured during the resting state. To quantify this, five symmetrical bins surrounding each peak are utilized to calculate the average power of both noise and the signal as follows

$$P_{noise} = \frac{\sum_{k=I_{noise-2}}^{I_{noise+2}} 10^{bins(k)} \cdot Freq(k)}{\sum_{k=I_{noise-2}}^{I_{noise+2}} Freq(k)} \quad (13)$$

$$P_{signal} = \frac{\sum_{k=I_{signal-2}}^{I_{signal+2}} 10^{bins(k)} \cdot Freq(k)}{\sum_{k=I_{signa-2}}^{I_{signal+2}} Freq(k)} \quad (14)$$

where I_{noise} and I_{signal} are the serial numbers of the bins corresponding to the noise peak center and the signal peak center respectively. And $Freq(k)$ is the frequency corresponding to the k-th bin. The SNR of the EMG signal is then obtained through the following equation

$$SNR_{EMG} = 10log_{10}^{\frac{P_{signal}-P_{noise}}{P_{noise}}} \quad (15)$$

Supplementary Note 3. The structure, mechanical properties, and electrophysiological signals of the BIH.

Supplementary Fig. 1 illustrates the molecular structures of both artificial ion channels. The negatively charged sulfonate groups on the zwitterionic side chains of pSBMA constructed cation channels in the BIH. And the positively charged quaternary ammonium groups on the zwitterionic side chains constituted anion channels in the BIH. Supplementary Fig. 2 displays the molecular structures of the hydrogen bond between the pSBMA and alginate. The hydrogen bonds can be formed between the hydroxyl group of alginate and acyl oxygen of pSBMA. Supplementary Fig.3a shows a schematic illustration of the tearing test. A standardized method is used to evaluate the toughness of hydrogels by quantifying their resistance to crack propagation under tension. Hydrogel samples are prepared in a trouser-shaped geometry with a pre-cut notch at the center to act as an initial crack. During the test, tensile force is applied to the two branches of the trouser-shaped sample, resulting in the crack propagates along the predefined path. Supplementary Fig. 3b presents a representative force versus extension curve of tearing test for the pSBMA based hydrogel and BIH. It can be seen that the addition of calcium alginate increases the toughness of BIH. Supplementary Fig. 4 shows tensile relaxation tests of the BIH at 100% strain for 1000 cycles, which reveals the excellent fatigue resistance of the BIH. The fracture strength of the BIH with different LiCl content was also investigated as illustrated in Supplementary Fig. 5. The fracture strength of BIH ranged from 9.6 to 12.3 kPa with the LiCl content increased from 0.63 to 3.07 wt%, indicating that LiCl has little effect on its breaking strength. A continuous ECG signal was recorded through the BIH electrode for 10 min, as presented in Supplementary Fig. 6a. The detailed heart rate information was extracted

from the ECG signal (Supplementary Fig. 6b), which showed average heart rate ranging from 77 to 81 bpm. The BIH is also capable of recording EMG signals generated during the bending of different fingers, as shown in Supplementary Fig. 7. It indicated that the BIH can accurately acquire EMG signals from subtle muscle activities.

Supplementary Note 4. The biocompatibility and degradability of the BIH.

The calcein-AM/PI double staining method was used to study the HACAT cells morphological evolution of living and dead cells of HACAT cells cultured in complete medium containing 0 μg/mL and 5000 μg/mL hydrogel leachate, as shown in Supplementary Fig. 9. The fluorescent images reveal that HACAT cells exhibited normal behavior and achieved higher densities with typical circular or elliptical morphologies over 24 to 72 h. There are no significant differences in morphology, distribution, or density were observed between the experimental and control groups. The apoptosis analysis of the control groups is shown in Supplementary Fig. 10. The Annexin V-FITC and PI staining solution were used in flow cytometry analysis to quantify both early and late apoptotic cells, and then distinguish viable cells from those undergoing apoptosis or necrosis. It reveals that no obvious differences in apoptotic levels compared to the experimental groups treated with the BIH. The results demonstrated that the proportion of apoptotic cells in the BIH-treated groups was comparable to that of the control groups, indicating that the BIH did not induce excessive apoptotic responses in the cellular population. The BIH can be completely degraded in PBS buffer, as shown in Supplementary Fig. 11. This degradation characteristic reveals the degradability of BIH in a simulated physiological environment.

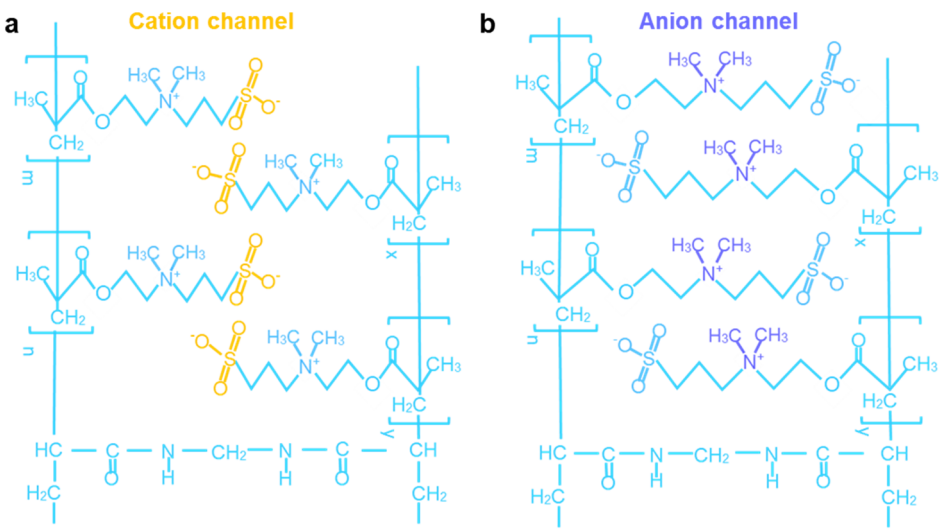

Supplementary Figure 1. Molecular structure diagram of the artificial (a) cation channel and (b) anion channel constructed by sulfonate groups and quaternary ammonium groups of the pSBMA.

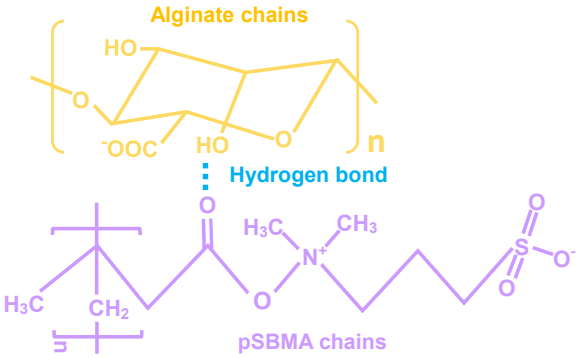

Supplementary Figure 2. Molecular structure diagram of the hydrogen bond between the pSBMA and alginate chains.

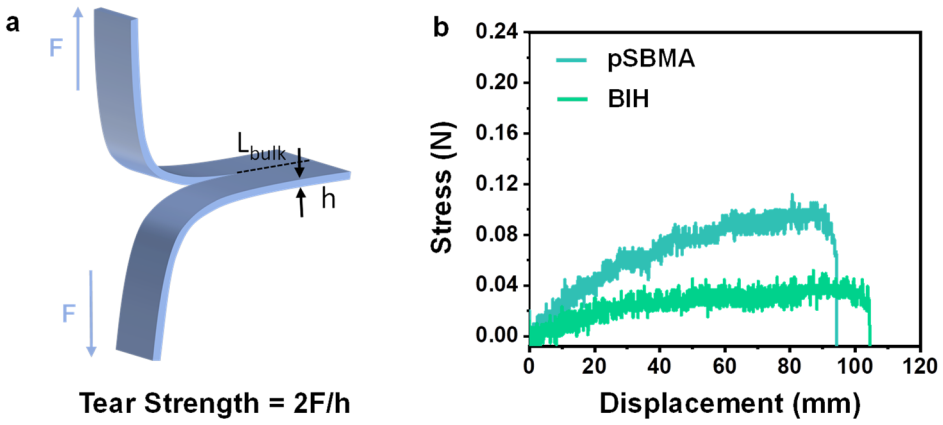

225

226 **Supplementary Figure 3. (a) Schematic illustration of the tearing test to quantify**
227 **the hydrogels' toughness. (b) Representative force versus extension curve of**
228 **tearing test for BIH and the pSBMA based hydrogel.**

229

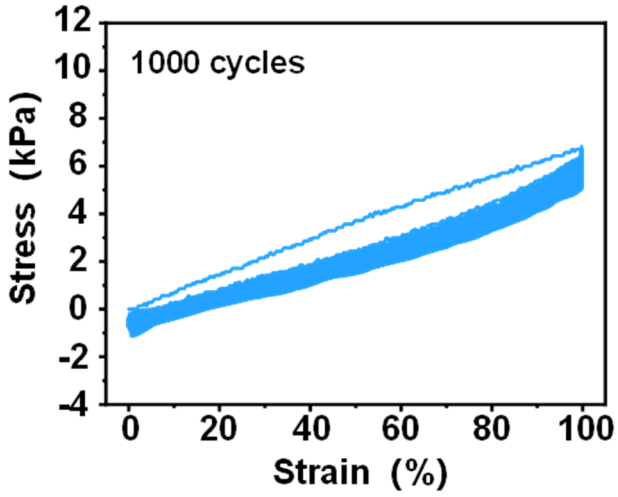

230

231 **Supplementary Figure 4. Tensile relaxation test of the BIH at 100% strain for 1000**
232 **cycles.**

233

234

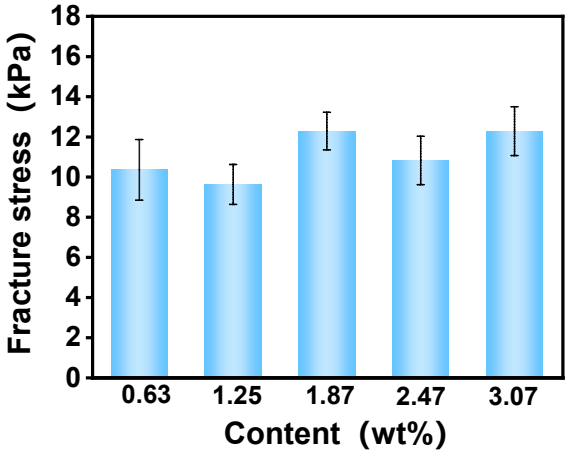

235

236 **Supplementary Figure 5. Fracture strength of BIH with different LiCl content.**

237 **The results are reported as their means ± SDs (N = 3 for independent samples).**

238

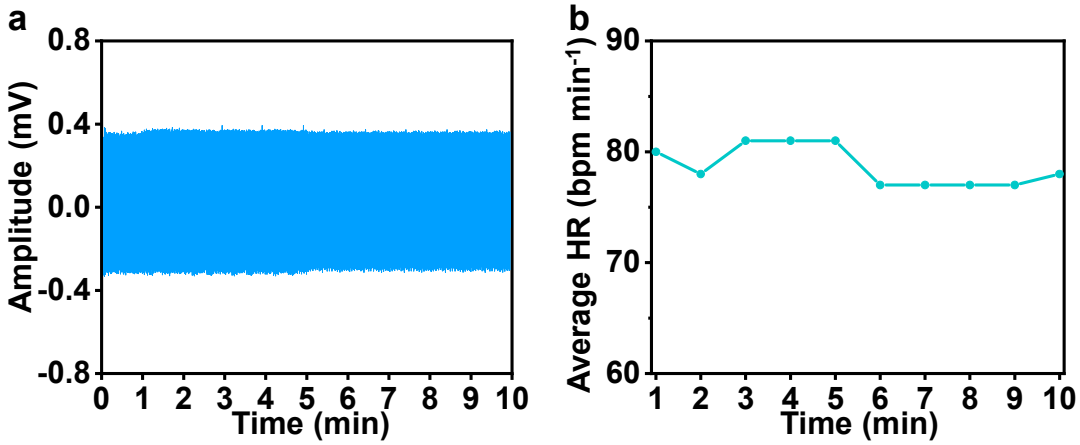

239

240 **Supplementary Figure 6. (a) The ECG signals lasting for 10 min acquired by the**

241 **BIH electrode. (b) The corresponding average heart rate per min calculated from**

242 **ECG signals**.

243

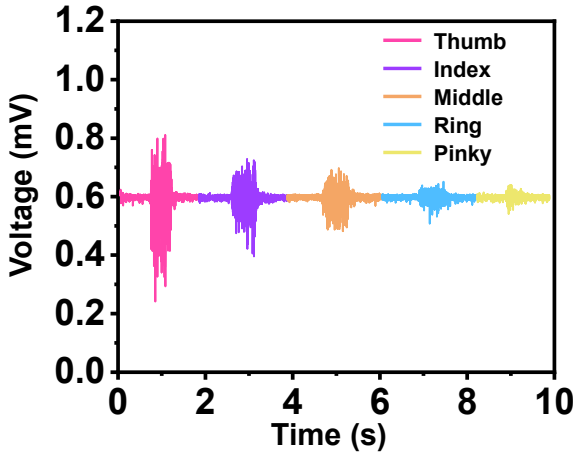

244

245 **Supplementary Figure 7. EMG signals recorded by the BIH electrode when**

bending different fingers.

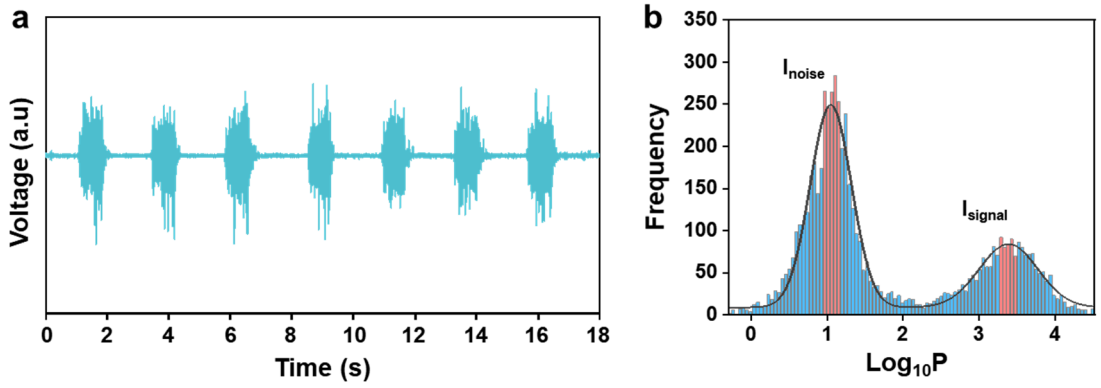

Supplementary Figure 8. (a) The EMG signals collected by the BIH electrode. (b) Signal and noise levels of the obtained EMG signals.

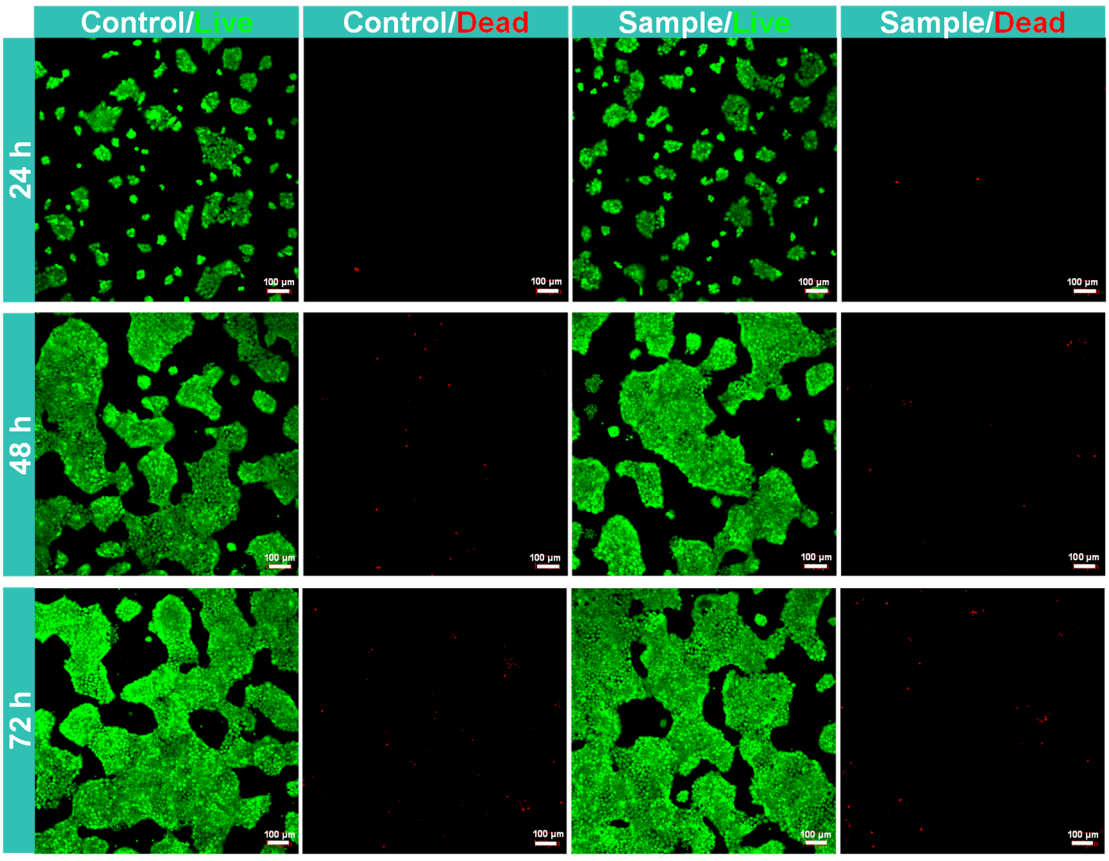

Supplementary Figure 9. Fluorescence microscope images of morphological evolution of living and dead cells of HACAT cells cultured in complete medium containing 0 ug/ml and 5000 ug/ml sample extracts for 24 h, 48 h, and 72 h.

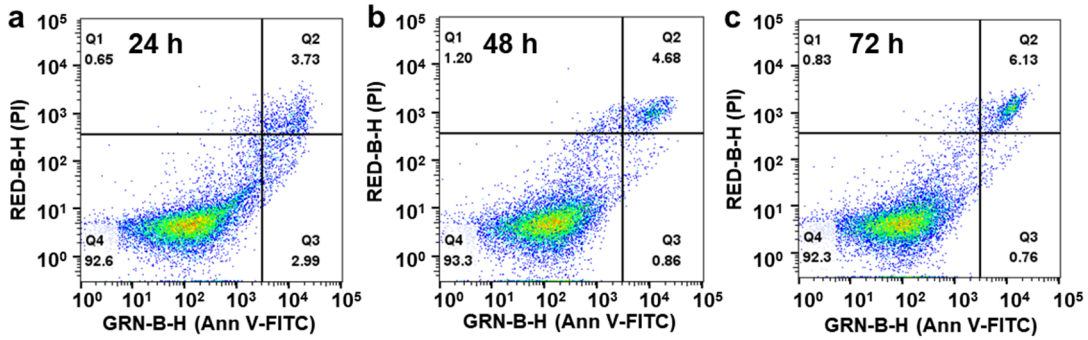

Supplementary Figure 10. **Apoptosis tests of HACAT cells cultured in complete medium containing 0 ug/ml sample extraction solution for (a) 24 h, (b) 48 h and (c) 72 h.**

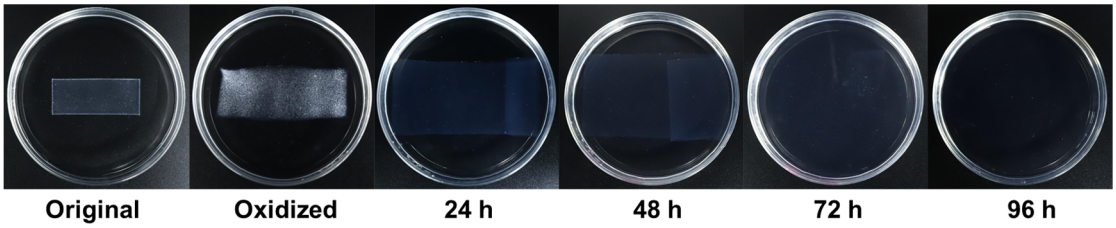

Supplementary Figure 11. The photographs of the degradation processes of BIH after oxidation and immersion in the PBS solution for 96 h.

Supplementary Table 4. A comparison of the BIH with other representative reported biomaterials based ionic hydrogels in terms of ionic conductivity and Young's modulus.

Biomaterials-based ionic Hydrogels	Conductivity (m S^{-1})	Young's modulus (kPa)	Ref.
BIH	7.04	7.2	This work
PHA/x-CS	0.0195	13.3	30
PAM/SA	0.0038	270	31
P(AM-co-AA)/HACC	2.16	420	32
PVA@HACC@HA	0.15	150	33

Starch/PVA/Gly/Na_3Cit	1.47	8850	34
PVA/cellulose	1.17	360	35
PAAm/Gelatin/ Ammonium sulfate	1.259	177	36
PVA/ADSP	1.93	950	37

271